NUMERICAL SIMULATION OF TYPHOON SURGES ALONG THE EAST COAST OF ZHEJIANG AND JIANGSU PROVINCES

Chen Changsheng (陈长胜) and *Qin Zenghao* (秦曾灏)

Shandong College of Oceanology, Qingdao

Received December 5, 1983

ABSTRACT

Using conventional two-dimensional nonlinear storm model, the storm surges caused by the six typhoons with different kinds of tracks which hit the coast of Zhejiang and Jiangsu Provinces including Shang-hai during the period from 1953 to 1974 are computed numerically. To avoid the nonlinear and linear computational instabilities, a finite-difference scheme with the quadratic conservation (or the semi-momentum) is adopted and a criterion for linear computational stability is derived. The basic parameters used in this computation are: the space step $\Delta s=30$ km, the time step $\Delta t=200$ sec, the coefficient of the wind stress $\nu_a^2=2.6\times10^{-3}$ and the coefficient of the bottom friction $\nu_b^2=2.0\times10^{-3}$. The pressure and surface wind distribution for typhoon are assumed to be characterized by Fujita's pressure formula and Ueno's wind model, respectively.

I. INTRODUCTION

Zhejiang and Jiangsu Provinces, which are situated in the east of China, own vast continental shelves and long coast line. The configuration of the whole sea region is rather complicated. Generally speaking, the sea bottom topography rises northwestward continueously, the slope of which in the direction normal to the coast is larger than that parallel to the coast. The depth of most parts of the sea region are within 100 m. The depth in the coastal region is less than 20 m, while the mean depth of the Hangzhou Bay is about 8 m. According to Ref. [1], the sea region of Zhejiang and Jiangsu Provinces near the coast should belong to the category of the shallow water theory of storm surges.

The coast of Zhejiang and Jiangsu Provinces, including Shanghai, is often hit by typhoons and is one of the regions which suffer more frequently from the surge disasters.

It is quite necessary to study typhoon surges dynamically in this region and develop a successful forcasting method. This paper just relates the very first attempt in this respect.

In the numerical computations for typhoon (or hurricane) surges, two-dimensional numerical models have been adopted widely, such as those developed by Miyazaki[2,3], Ueno[4], Jelesnianski[5-8] and Johns[9,10]. From the point of view of computational mathematics, all these models are linear except Johns'.

Although Ueno took account of the nonlinear advective terms in his work, he used the successive linearization for them at intervals of a certain number of time steps to avoid the nonlinear computational instability. In fact, he regarded the effect of the nonlinear advective terms as a correction to the linear model. More specifically, it still belongs to a linear model. Using the nonlinear dynamical models results in the problem of the nonlin-

ear computational stability. However, in the numerical simulation for typhoon surges, this point has not been taken into account.

In order to overcome the deficiencies of the models mentioned above, a finite difference scheme with the quadratic conservation is introduced into the numerical computations for typhoon surges striking the coast of Zhejiang and Jiangsu Provinces including Shanghai. We, for example, have successfully simulated the six typhoon surges with different kinds of tracks and described the whole process (i. e., genesis, development and disappearance) of the typhoon surge.

II. DYNAMICAL MODEL

The Typhoon surge under consideration is a phenomenon of the large-scale geophysical fluid dynamics, i. e., the horizontal scale of meteorological disturbances generating storm surges is much greater than the water depth. According to this characteristic of "boundary layer" current field, three-dimensional equations of motion and continuity may be integrated over the depth of the sea and yield:

$$\frac{\partial u}{\partial t}+u\frac{\partial u}{\partial x}+v\frac{\partial u}{\partial y}-fv=-g\frac{\partial \xi}{\partial x}-\frac{\partial p_a}{\partial x}+\frac{\rho_a v_a^2|\boldsymbol{W}|w_x}{\rho(\xi+h)}-\frac{v_b^2|\boldsymbol{V}|u}{(\xi+h)}, \tag{1}$$

$$\frac{\partial v}{\partial t}+u\frac{\partial v}{\partial x}+v\frac{\partial v}{\partial y}+fu=-g\frac{\partial \xi}{\partial y}-\frac{1}{\rho}\frac{\partial p_a}{\partial y}+\frac{\rho_a v_a^2|\boldsymbol{W}|w_y}{\rho(\xi+h)}-\frac{v_b^2|\boldsymbol{V}|v}{(\xi+h)}, \tag{2}$$

$$\frac{\partial \xi}{\partial t}+\frac{\partial}{\partial x}[(\xi+h)u]+\frac{\partial}{\partial y}[(\xi+h)v]=0. \tag{3}$$

The boundary conditions are assumed to be

1. $\boldsymbol{V}=0$, at the coastal boundary

2. $\xi=\frac{10^3}{\rho g}(\rho_\infty-p_a)$, at the open boundary and the initial conditions are

$$u=v=0, \quad \xi=\frac{10^3}{\rho g}(p_\infty-p_a), \quad \text{at} \quad t=0.$$

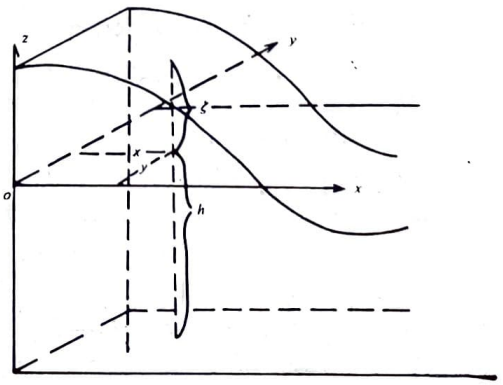

Fig. 1. The coordinate system.

III. NUMERICAL MODEL

1. *Finite-difference Scheme*

With the step Δt along the time-axis and Δs along x and y axes (Fig. 2), we can make Eqs. (1)—(3) discrete and obtain the corresponding finite-difference equations used for computation as follows[11]:

$$\bar{u}_t^t=-\overline{\bar{u}^x u_x}^x-\overline{\bar{v}^y u_y}^y+fv_{i,j}^n-g\bar{\xi}_x^x-\frac{1}{\rho}\bar{p}_{ax}^x+\frac{\rho_a v_a^2|\boldsymbol{W}|_{i,j}^n w_{i,j}^n}{\rho D_{i,j}^n}-\frac{v_b^2|\boldsymbol{V}|_{i,j}^{n-1}u_{i,j}^{n-1}}{D_{i,j}^n}, \quad (4)$$

$$\bar{v}_t^t=-\overline{\bar{u}^x v_x}^x-\overline{\bar{v}^y v_y}^y-fu_{i,j}^n-g\bar{\xi}_y^y-\frac{1}{\rho}\bar{p}_{ay}^y+\frac{\rho_a v_a^2|\boldsymbol{W}|_{i,j}^n w_{i,j}^n}{\rho D_{i,j}^n}-\frac{v_b^2|\boldsymbol{V}|_{i,j}^{n-1}v_{i,j}^{n-1}}{D_{i,j}^n}, \quad (5)$$

$$\bar{\xi}_t^t=-(\bar{D}^x\bar{u}^x)_x-(\bar{D}^y\bar{v}^y)_y. \quad (6)$$

Let α be an arbitrary variable (such as u, ξ, p_a, etc.), the operators in Eqs. (4)—(6) can be defined as:

$$\overline{\bar{u}^x\alpha_x}^x=\frac{1}{4\Delta s}[(u_{i,j+1}^n+u_{i,j}^n)(\alpha_{i,j+1}^n-\alpha_{i,j}^n)+(u_{i,j}^n+u_{i,j-1}^n)(\alpha_{i,j}^n-\alpha_{i,j-1}^n)], \quad (7)$$

$$\overline{\bar{v}^y\alpha_y}^y=\frac{1}{4\Delta s}[(v_{i+1,j}^n+v_{i,j}^n)(\alpha_{i+1,j}^n-\alpha_{i,j}^n)+(v_{i,j}^n+v_{i-1,j}^n)(\alpha_{i,j}^n-\alpha_{i-1,j}^n)], \quad (8)$$

$$(\bar{D}^x\bar{u}^x)_x=\frac{1}{4\Delta s}[(u_{i,j+1}^n+u_{i,j}^n)(D_{i,j+1}^n+D_{i,j}^n)-(u_{i,j}^n+u_{i,j-1}^n)(D_{i,j}^n+D_{i,j-1}^n)], \quad (9)$$

$$(\bar{D}^y\bar{v}^y)_y=\frac{1}{4\Delta s}[(v_{i+1,j}^n+v_{i,j}^n)(D_{i+1,j}^n+D_{i,j}^n)-(v_{i,j}^n+v_{i-1,j}^n)(D_{i,j}^n+D_{i+1,j}^n)], \quad (10)$$

$$\bar{\alpha}_x^x=\frac{1}{2\Delta s}(\alpha_{i,j+1}^n-\alpha_{i,j-1}^n), \quad (11)$$

$$\bar{\alpha}_y^y=\frac{1}{2\Delta s}(\alpha_{i+1,j}^n-\alpha_{i-1,j}^n), \quad (12)$$

$$\bar{\alpha}_t^t=\frac{1}{2\Delta t}(\alpha_{i,j}^{n+1}-\alpha_{i,j}^{n-1}), \quad (13)$$

$$D_{i,j}^n=H_{i,j}+\xi_{i,j}^n, \quad (14)$$

$$H_{i,j}=0.25(h_{i+1,j}+h_{i-1,j}+h_{i,j-1}+h_{i,j+1}), \quad (15)$$

where $v_a^2=2.6\times10^{-3}$ and $v_b^2=2.0\times10^{-3}$.

The scheme given above is an explicit one and possesses the advantage of the quadratic conservation (or the semi-momentum) through which the nonlinear computational instability can be controlled. Its truncation error is easily derived as O ($(\Delta t)^2+(\Delta s)^2$).

2. *Linear Computational Stability*

The results of analyses, both theoretical and computational, show that there still exists a problem of linear computational instability depending on the choice of time and space steps in the nonlinear discrete equations. More specifically, a necessary condition for the stability of the nonlinear discrete equations is that the linearized perturbation equations should be stable. To solve this problem introducing the Fourier method into a system of linearized perturbation equations derived from Eqs. (1)—(3), we can easily obtain the criteria for linear computational stability as follows:

(1) for $F=0$ (i. e., the effect of bottom friction disappeares), the stability criterion can be reduce to

$$\sqrt{\alpha}\frac{\Delta t}{\Delta s}\left[|\boldsymbol{V}|+\sqrt{g\hat{D}}\left(1+\frac{1}{4}\left(\frac{f\Delta s}{\hat{C}}\right)^2\right)\right]\leqslant 1. \quad (16)$$

Eq. (16) agrees with the result given by Irvine and Houghton[12] (1970).

(2) for $f=0$ and $\boldsymbol{V}\cdot\nabla\boldsymbol{V}=0$ (i. e., both Coriolis force and nonlinear advective terms are assumed to be zero), a simple stability criterion can be derived approximately as follows:

$$\Delta t\hat{\beta}\Big/4\sqrt{\hat{D}g}\leqslant s<\frac{1}{\sqrt{2\hat{D}g}}, \tag{17}$$

where $s=\Delta t/\Delta s$.

Actually, in the numerical computations s is first chosen in such a manner that it may best suit the stable conditions given by Eqs. (16) and (17), and then determined by a number of numerical tests.

In the present paper the space step Δs is taken to be 30 km and the time step $\Delta t=200$ sec.

3. *Filtering Technique*

Owing to the errors arising from the boundary conditions, it is possible to produce some error short waves which lead to all the unstable computations. Accordingly, we have to eliminate these kinds of waves by employing a filter. In this work, the five-point space smoothing operator of the following form is adopted for each time step in order to avoid computational instability:

$$\bar{\alpha}_{i,j}=(1-\hat{s})\alpha_{i,j}+\frac{\hat{s}}{4}(\alpha_{i-1,j}+\alpha_{i+1,j}+\alpha_{i,j-1}+\alpha_{i,j+1}) \tag{18}$$

where $\hat{s}=0.5$.

The computational results in this paper show that this filtering technique is effective.

4. *Computations of Currents and Surges at Boundary Grids*

In the computations of the numerical models (4)—(6), the current and surge at a grid point are determined by their corresponding values at four neighbouring grid points. Obviously, such computations can not be applied to those at the boundary grid. For convenience, the following extrapolation formula is employed:

$$\left(\frac{\partial\alpha}{\partial n_b}\right)_M^{n+1}=\left(\frac{\partial\alpha}{\partial n_b}\right)_{M_1}^{n+1} \tag{19}$$

where n_b is the coordinate normal to the boundary, M,the boundary grid point, and M_1,the grid point next to M in the direction of n_b.

This extrapolation formula not only assures the computational stability of the currents and surges at the boundary grids, but also is very simple. The results of computations for typhoon surges show that this treatment is effective for the grid size of 30 km.

IV. METEOROLOGICAL CONDITIONS

1. *Computed Typhoons*

Based on the analyses of historical samples of the disastrous typhoon surges, six typhoons with different kinds of tracks which hit the coast of Zhejiang and Jiangsu Provinces including Shanghai during the period from 1953 to 1974 have been chosen for computation (see Fig. 3). They are the typhoons No. 5310, 5612, 6005, 6126, 6207 and 7413. All these typhoons caused intensive rise of sea level and the heavy surge disasters in these areas, especially the Hangzhou Bay. For example, the strong typhoon No. 5612, landed at Xiangshan County, Zhejiang Province in 1956, created the maximum surge (5.09) in the history of the tidal record in the East China Sea.

Since detailed observations about typhoon over the sea are hardly made, so we have

to treat a real typhoon as a model one by using an approximate method. In our computations, taking the observational records every six hours, the data of typhoons, such as its centre position, speed and centre pressue, are given at each time step by means of linear interpolation. At least, this approximate treatment is available for the processes of typhoons which move steadily during six hours.

2. *Computations of Pressure Field and Wind Field*

(1) *Distribution of pressure*

The pressure p_a at each grid point is calculated by Fujita's formula as follows:

$$p_a = p_\infty - (p_\infty - p_0)\Big/\sqrt{1+\left(\frac{r}{r_0}\right)^2}$$

where p_∞ and r_0 are assumed to be constants during all the typhoon's passage.

(2) *Distribution of wind field*

The wind distribution in the typhoon area is much more complicated than the pressure distribution. So for a model of the wind distribution which coincides perfectly with the real one has not been developed. In the numerical computations of typhoon surges, both Ueno's wind and Jelesnianski's wind field models are widely employed. Corresponding to Fujita's pressure model, Ueno's wind field model is adopted as our wind formula and may be:

$$\begin{pmatrix} W_x \\ W_y \end{pmatrix} = C_1 \begin{pmatrix} V_{x_0} \\ V_{y_0} \end{pmatrix} \exp\left(-\frac{r\pi}{5\times 10^7}\right) \mp C_2 \left(\sqrt{\frac{10^3 \Delta p}{\rho_a}}\,\frac{1}{r_0}\,z^{3/2} - \frac{f}{2}\right)\left[(x_i - x_0)\begin{pmatrix} \sin 30^\circ \\ \cos 30^\circ \end{pmatrix} \pm (y_i - y_0)\begin{pmatrix} \cos 30^\circ \\ \sin 30^\circ \end{pmatrix}\right], \tag{21}$$

where $z = \left(1+\left(\frac{r}{r_0}\right)^2\right)^{-\frac{1}{2}}$. r_0 is first obtained by calculating the mean radius of a referential isobar on a weather chart during all the typhoon's passage and then determined by a curve fitting technique of pressure at stations. The choices of C_1 and C_2 refer to [4] and [13]. In general, it is based on the principle that the computed curve of wind field agrees fairly well with the observed one. For all the typhoon's passage, C_1 and C_2 are assumed to be constants (Table 1).

Table 1 The Parameters for Typhoons

Parameter \ Typhoon	5310	5612	6005	6126	6207	7413
p_∞(hPa)	1010	1008	1005	1010	1005	1005
r_0(km)	92	98	85	96	177	137
C_1	6/7	6/7	6/7	6/7	6/7	4/7
C_2	0.62	0.62	1.33	0.62	1.33	0.7

V. REGION USED FOR COMPUTATION

In order to eliminate the influence of the open boundary conditions on the surge elevations, we selected a larger sea area as the computational region, the maximum dimensions of which are 660 km from 26°9′N to 32°45′N × 690 km from 119°48′E to 127°40′E (Fig. 2).

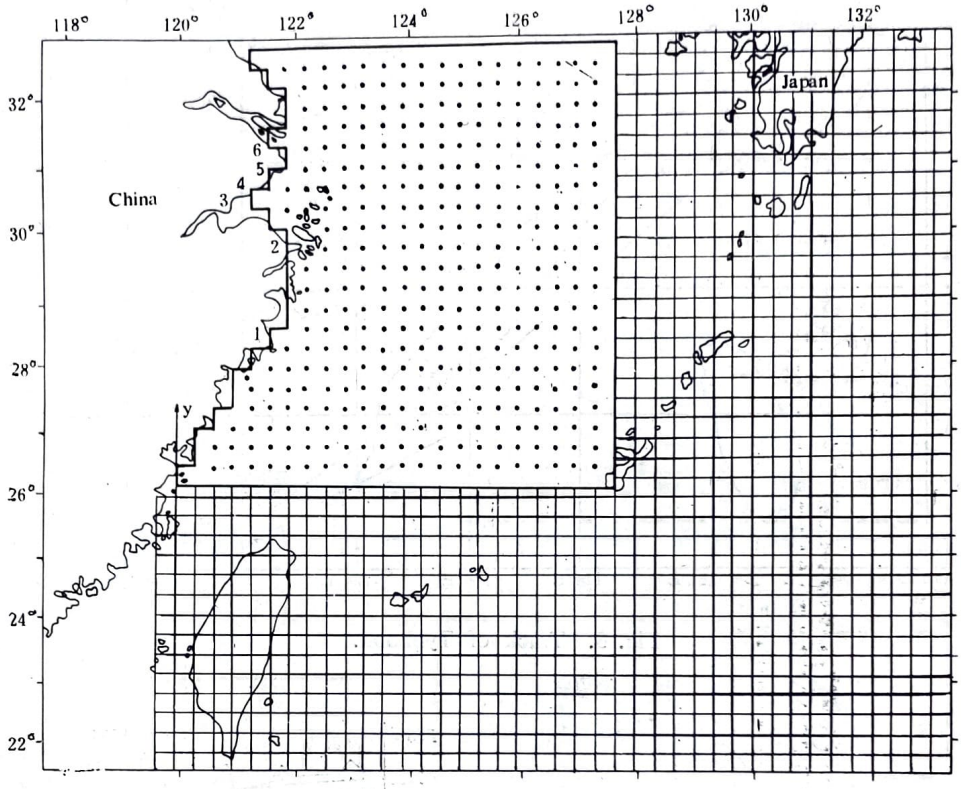

Fig. 2. The finite difference grid used in typhoon surge computations.
1—Haimen, 2—Zhenhai,
3—Ganpu, 4—Zapu,
5—Gingshan, 6—Wusong.

VI. RESULTS OF COMPUTATIONS AND DISCUSSIONS

1. *Simulations of Pressure and Wind Fields for Typhoon*

As examples, the comparisons between the observed and computed values of pressure and wind for three typhoons with different kinds of tracks at several stations are shown in Fig. 4. The main conclusions reached are as follows:

(1) The computed results of pressure, such as its variation trend and magnitude, are in good agreement with the observations.

(2) The error between the computed and observed values of pressure for alongshore travelling typhoons is smaller than that for land-falling typhoons.

(3) The computed wind direction coincides fairly well with the observational ones.

The results obtained by simulating the other typhoon processes are similar to those shown above at stations.

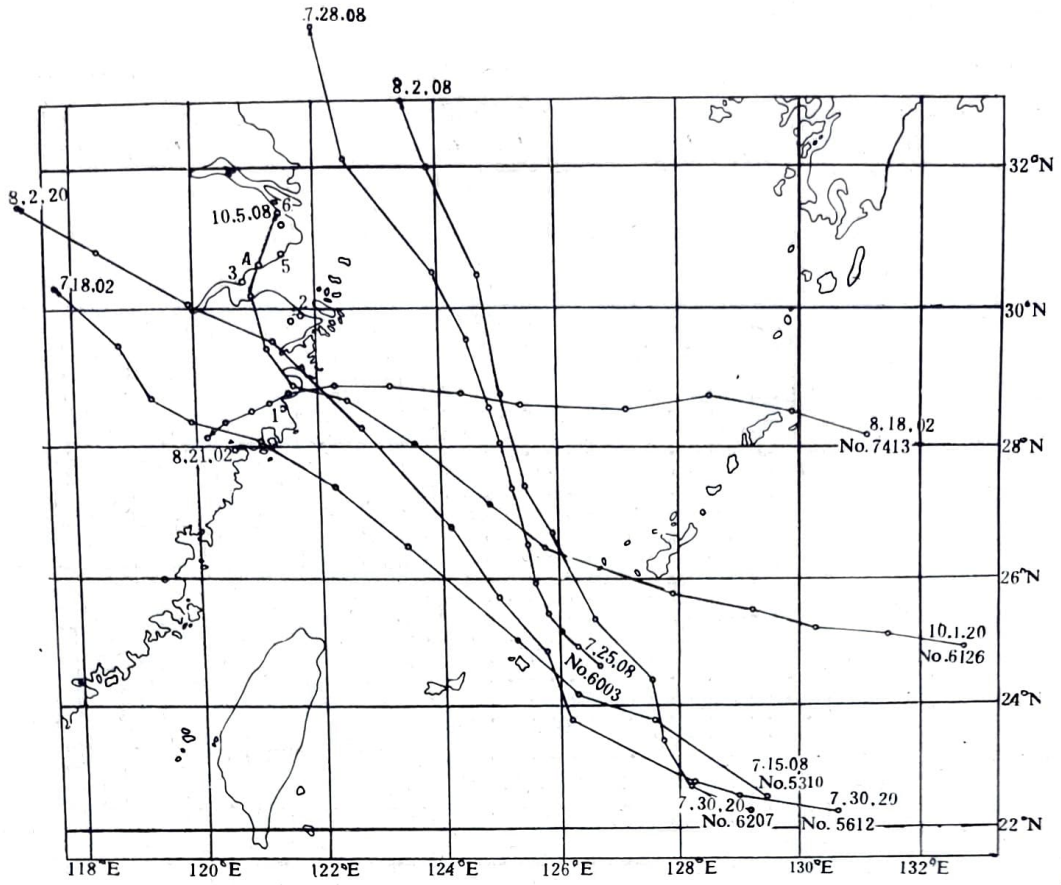

Fig. 3. Track of Typhoon.

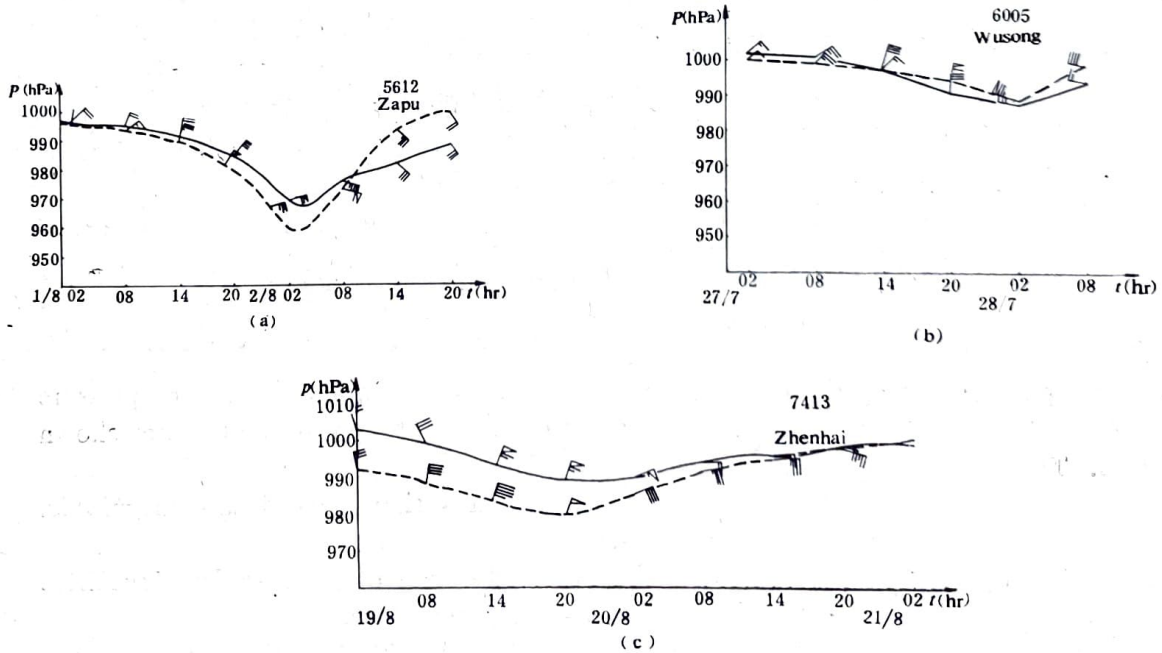

Fig. 4. Comparisons between the observed and computed values of pressure and wind fields.
—— Observed pressure; - - -Computed pressure.

2. *Simulation of Surge Elevation*

At first, it is necessary to present the sources of the observed data of surge elevation, because it is closely related to the choice of the standards of comparison in numerical computation. In this paper, two different kinds of methods are used: (1) subtraction of the predicted tides consisting of 128 constituents from the recorded water level. (2) Subtraction of the predicted tides consisting of 60 constituents from the recorded water level. As compared with the curves of surge elevation obtained by the former method, most of those obtained by the latter method are found to show more or less pronounced secondary oscillations with semi-diurnal or shorter tidal periods. In addition to the nonlinear couping between tide and storm surge, the influence of the accuracy of predicting tide on the results of separating elevation is not negligible. On the basis of unchanging the trend of variation of surge elevation and affecting the maximum elevation as less as possible, the five-hourly averages are used to smooth the curves with semi-diurnal or shorter tidal periods.

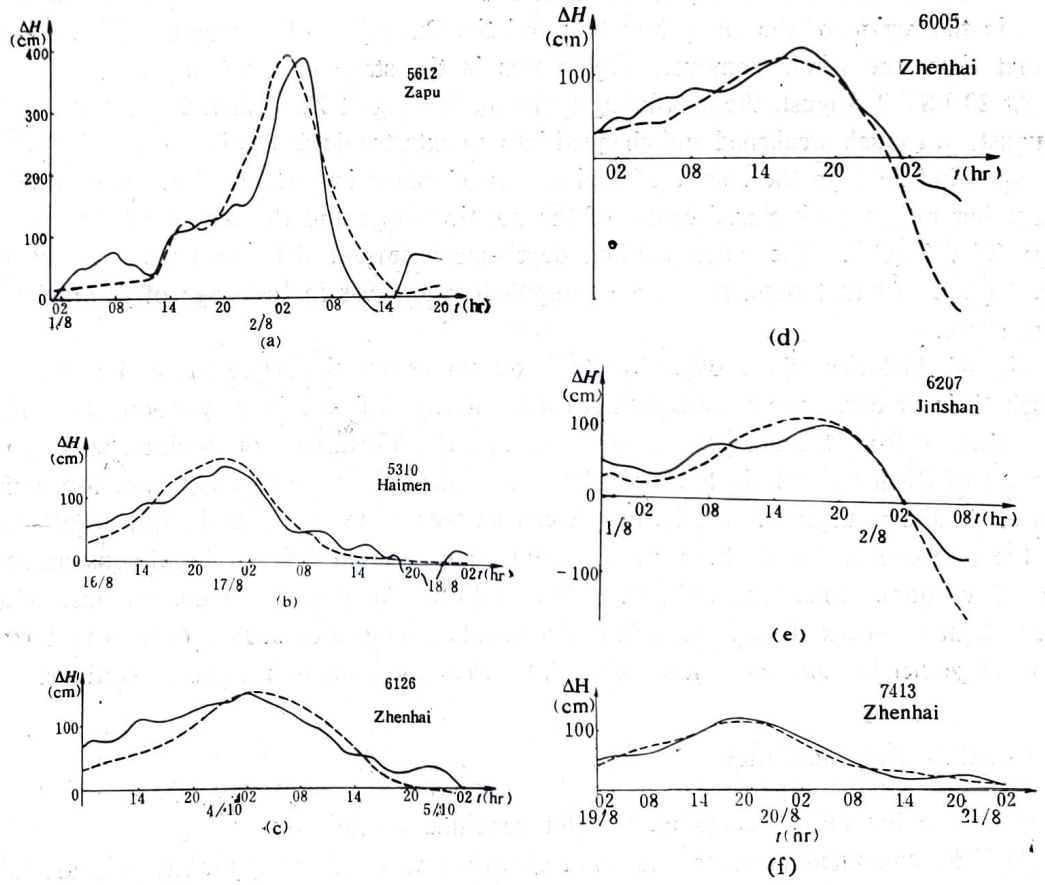

Fig. 5. Comparisons between the observed and computed surges.
—— Observation; - - - Computation.

As examples, Fig. 5 shows the comparisons between the observed and computed values of surge elevation for three typhoon processes with different tracks at some stations. The main features are as follows:

(1) The trend of variation of observed and computed surge in every typhoon process is analogous to each other.

(2) The computed surges agree fairly well with observations. The difference between them is within 23 cm.

(3) For every typhoon, the phase difference between the observed and computed peak surges is within two hours.

The results of simulation for other typhoon surges are that all stations rose obviously, the amount of which was larger in the south than that in the north (Fig. 7 (a)). At the same time, the depth-mean current in this region flowed from east to west and was divided into two branches near the coast, one moved northward and resulted in a clockwise circulation, the other moved southward and formed a counterclockwise circulation. In the south of Haimen, there existed a strong stream, strengthened southward (Fig. 6 (a)), at that time, the whole computed region was in the stage of forerunner of storm surge.

At 20 LST 1 August, the strong typhoon approached near the coast and continued moving northwestward. The water level in the whole computed region rose rapidly and the ascent of their isopleths veered from south to west. The centre of maximum water level not only reached the vicinity of the Hangzhou Bay but also strengthened greatly (Fig.7(b)). Moreover, there were the strong depth-mean water mass transports coming from the outer ocean in the region of the Hangzhou Bay and the Changjiang River mouth (Fig. 6 (b)). At that time, the whole computed region was in the stage of main surge.

At 20 LST 2 August, the landfalling typhoon, landing at Xiangshan County at 24 LST 1 August, was much weakened and changed into an extratropic depression. The effect of the typhoon wind field on the computed region was of minor importance, but there remained a large but rather weak closed centre of the positive surge and the region of the negative surge (Fig. 7 (c)). The corresponding depth-mean current field weakened remarkably (Fig. 6 (c)). At that time, the whole computed region was in the stage of resurgence of storm surge.

The life histories of the other five typhoon surges are similar to those shown above though their tracks, speeds, and strength are utterly different from typhoon No. 5612's.

It follows from the analyses given above that the life history of typhoon surge along the coast of Zhejiang and Jiangsu Provinces experiences three main stages, i. e. forerunner, main surge and resurgence. In addition, it can be seen from Fig. 3 and Figs. 6 (a)—6 (c) that the response of the depth-mean current field to the wind field of typhoons needs to take a few hours. In other words, there is an adjustment process in the response of the sea to the atmospheric disturbances. It is due to the existance of such a process that maximum surge height appears a few hours later than the maximum wind at stations.

VII. CONCLUDING REMARKS

From the foregoing discussion, we can conclude as follows:

(1) The computed pressure and wind direction fields of the typhoons coincide fairly well with the observed ones, respectively.

(2) The computed surges are in good agreement with the observed ones.

(3) The computed surges reflect, both quantitatively and qualitatively, the actual conditions of the six typhoon surges hitting the coast of Zhejiang and Jiangsu Provinces.

Finally, it should be pointed out that the computed model wind speeds are not satisfactory at several stations. There is a marked difference between the observed and computed wind speeds. This means that Ueno's wind field model needs further revising. However,

it is worth noting that the errors caused by the model wind speed are of less influence on the whole computed results of typhoon surges, although they reflect more or less in the errors of simulating water level. In fact, the rising of local water level is not determined instantly by local wind speed but depends on the time-integrated effect of the horizontal distribution of regional wind stress. Therefore, we may deduce that the very similar to those given above. It follows that the computed results reflect, both quantitatively and qualitively, the actual conditions of the six typhoon surges which hit the coast of Zhejiang and Jiangsu Provinces.

3. *Life History of Typhoon Surges*

To clearly indicate the whole process of the typhoon surge (i. e, genesis, development

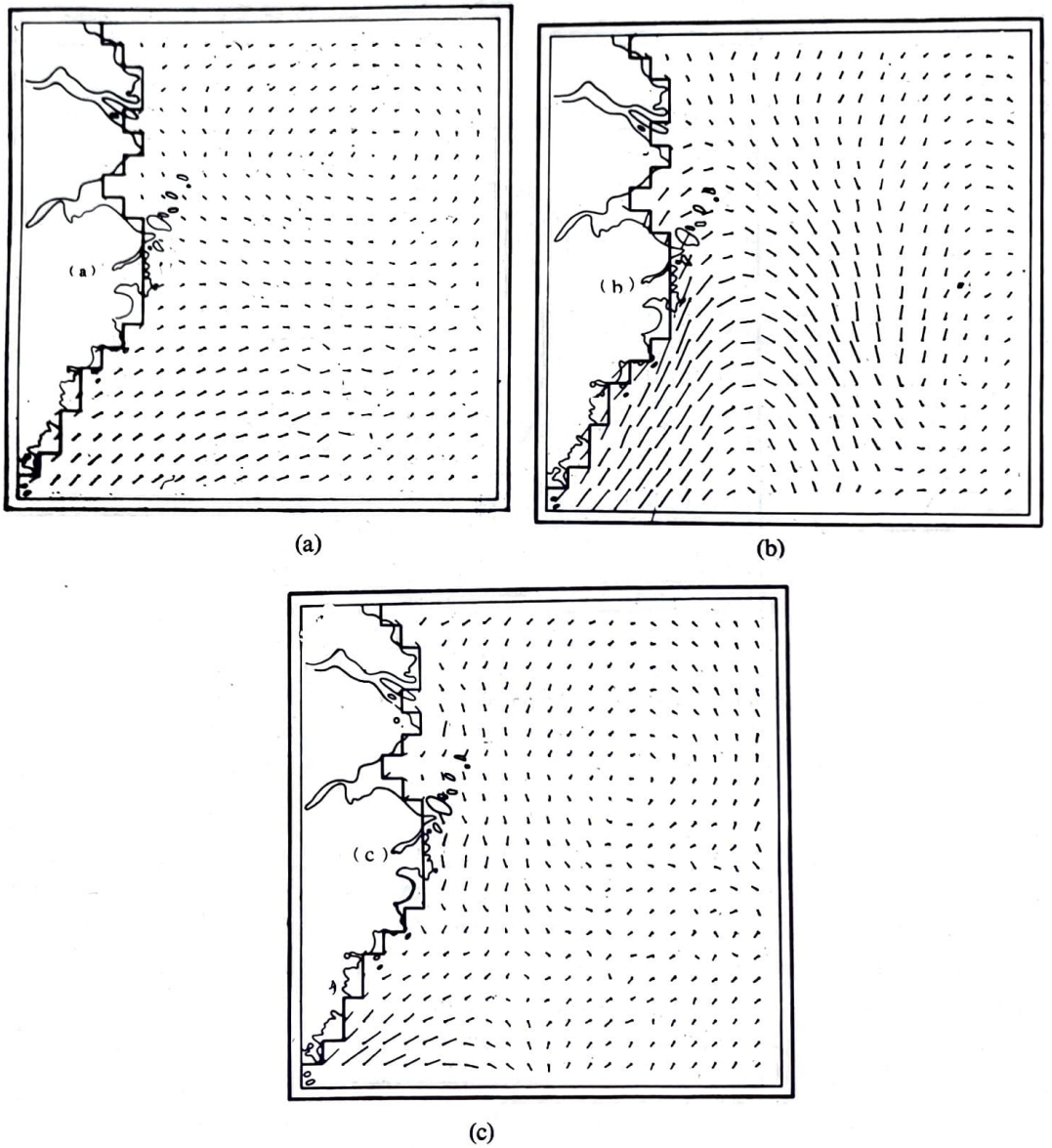

Fig. 6. Computed depth-mean current vectors.
(a) 02 LST 1 Aug. 1956; (b) 20 LST 1 Aug. 1956;
(c) 20 LST 2 Aug. 1956,

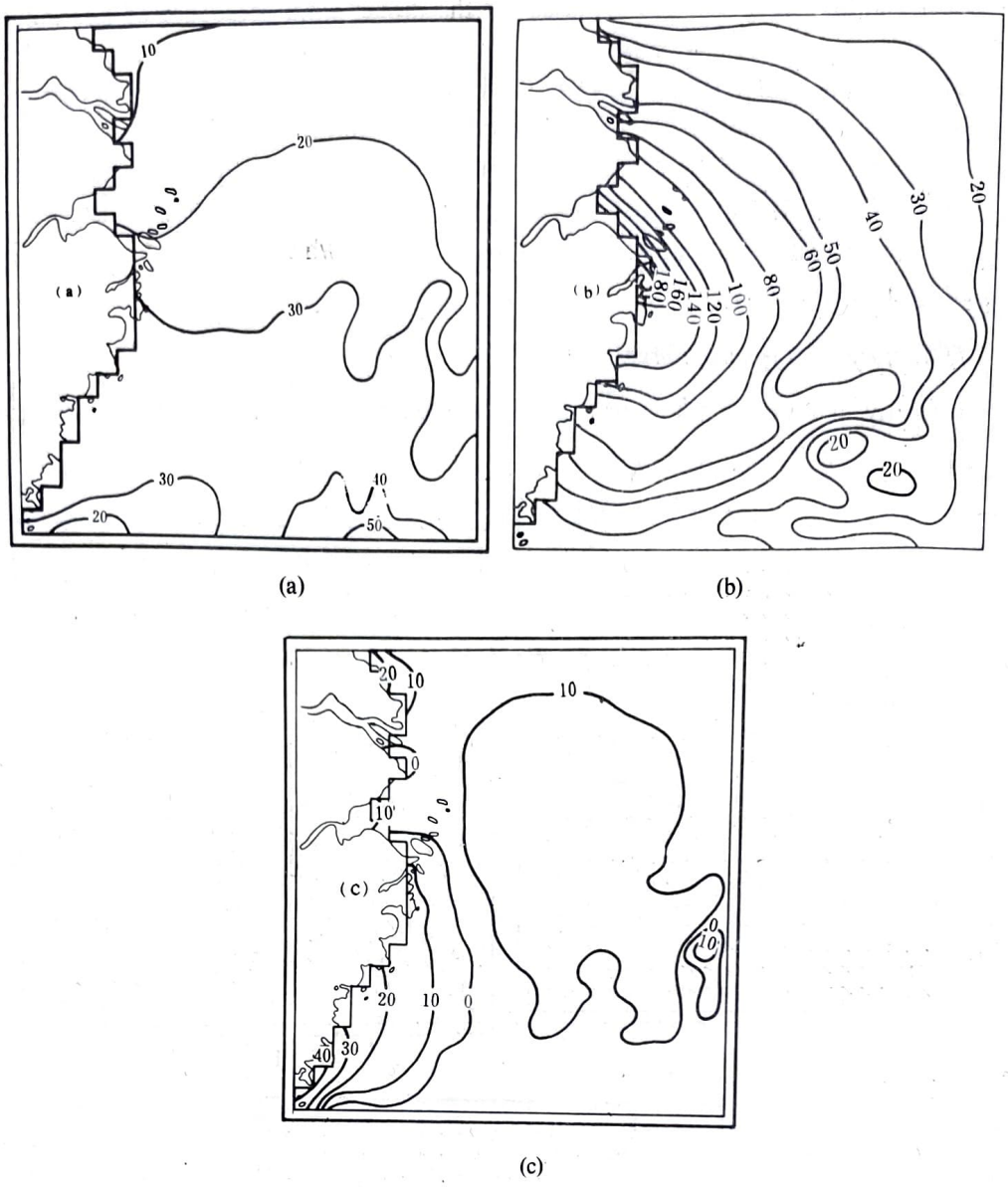

Fig. 7. Distributions of the Computed surges (cm).
(a) 02 LST 1 Aug. 1956; (b) 20 LST 1 Aug. 1956;
(c) 20 LST 2 Aug. 1956.

and disappearance), the storm surge caused by the strong typhoon No. 5612 is taken as an example and some main features during its life history are discussed. Figs. 6 (a)—6 (c) and Figs. 7(a)—7(c) show the calculated distributions of water level and depth-mean current of the typhoon surge, respectively. Combining these figures with Fig. 3, we can see that at 02 LST 1 August, although the strong typhoon was still located at the open ocean far from the computed region, the forerunner of swell propagating along the coast from south to north appeared on the the computed region. The water level at typhoon surges are more sensitive to local wind direction compared with local wind speed. In other words, the accurate simulation of the wind direction is more important than that of the wind speed in regard to their influences on typhoon surges. Of course, whether this deduction is true or not needs to be justified by the experiments for model typhoons.

LIST OF SYMBOLS

C_1, C_2 proportional coefficients of field wind and gradient wind, respectively;
$\hat{C}=\sqrt{g\hat{D}}$ characteristic value of phase velocity of long gravity wave;
$D=h+\xi$ total depth of the water;
$\hat{D}$ characteristic value of D;
f Coriolis parameter;
g acceleration of gravity;
$h=h\ (x, y)$ undisturbed depth of the water;
i index parameter in y direction, i. e. $y=i\,\Delta y$.
j index parameter in x direction, i. e. $x=j\Delta x$;
n index parameter in time axis, i. e. $t=n\Delta t$;
p_a atmospheric pressure;
p_0 pressure in the centre of the typhoon;
p_∞ ambient atmospheric pressure of the typhoon; $\Delta p=p_\infty-p_0$;
$r=\sqrt{(x_i-x_0)^2+(y_i-y_0)^2}$ distance from any grid point to the centre of the typhoon;
r_0 constant of typhoon;
t time;
u, v components of the depth-mean current in x and y directions, respectively;
$|\hat{v}|$ characteristic value of U and V.
V_{x_0}, V_{y_0} compontents of the typhoon's speed in x and y directions, respectively;
x, y horizontal components of right-hand coordinates, (x, y)-plane lie on the undisturbed water surface with x eastward and y northward (Fig. 1).
w_x, w_y compontents of sea surface wind in x and y direction , respectively.
$\hat{\beta}$ friction coefficient;
ρ density of the water, $\rho=1.025$ g/cm^3;
ρ_a density of air, $\rho_a=1.2929\times10^{-3}$ g/cm^3;
$\xi=\xi\ (x, y)$ elevation of the sea surface;
ν_a^2 coefficient of the wind stress;
ν_b^2 coefficient of the bottom friction.

REFERENCES

[1] Chin Tsenghao (Qin Zenghao) & Feng Shihzao (Feng Shizuo), *Scientia Sinica*, **18**(1975), 2: 241—261.
[2] Miyazaki, M. et al., *Oceanograal. Mag.*, **13**(1961), 1:51—75.
[3] Miyazaki, M. et al., *Oceanograal. Mag.*, **13**(1962), 2:103—107.
[4] Ueno, T., *Oceanograal. Mag.*, **16**(1964), 53—124.
[5] Jelesnianski, C. P., *Mon. Wea. Rev.*, **93**(1965), 6:343—358.
[6] Jelesnianski, C. P., *Mon. Wea. Rev.*, **94**(1966), 6:379-394.
[7] Jelesnianski, C. P., *Mon. Wea. Rev.*, **95**(1967), 11:740—756.
[8] Jelesnianski, C. P., *NOAA, AM. NWS. TDL*-46, 1972, 52.
[9] John, B., *Monsoon Dynamics*, New Delhi, 1977, 689—705.
[10] John, B. & Ali, Anwar, *Quart. J. R. Met. Soc.*, **106**(1980), 1—18.
[11] Arne, G., *Mon. Wea. Rev.*, **97**(1969), 5:384—404.
[12] William, S. Irvine, Jr, & David D. Houghton, *Mon Wea. Rev.*, **99**(1970), 8:606—616.
[13] 吴培木等，海洋学报，**3**(1981), 1:28—43.